THE JOURNAL OF CHEMICAL PHYSICS **133**, 084502 (2010)

Quantum-classical description of environmental effects on electronic dynamics at conical intersections

Aaron Kelly[a] and Raymond Kapral[b]
Department of Chemistry, Chemical Physics Theory Group, University of Toronto, Toronto, ON M5S 3H6, Canada

(Received 29 March 2010; accepted 16 July 2010; published online 23 August 2010)

Quantum-classical Liouville theory is used to simulate the dynamics of systems containing conical intersections. In particular quantum dynamical effects on the electronic population transfer and coherence in a quantum subsystem that arise from the presence of an environment are studied. The environment, in turn, is partitioned into an immediate environment representing, say, local molecular vibrations, and a bath representing other degrees of freedom. Population transfer may be enhanced or suppressed, depending on the relative values of the characteristic frequencies of the immediate environment and bath. Electronic decoherence and the destruction of geometric phase effects were observed for bath frequencies that are large relative to the molecular vibrations. The dynamics at higher dimensional conical intersections was found to be very sensitive to the environmental coupling. When a single collective solvent coordinate couples directly to the electronic subsystem, the characteristic frequency of the new coordinate, relative to that of the nuclear vibrational modes, has a strong effect on the population dynamics. The results also serve as a test of the QCL dynamical scheme for future applications to more detailed molecular descriptions of condensed phase environments for conical intersection dynamics. © *2010 American Institute of Physics*. [doi:10.1063/1.3475773]

I. INTRODUCTION

Conical intersections exist within the potential energy landscapes of many molecular systems.[1–4] Although systems containing conical intersections (CIs) have been studied with increasing intensity for more than 70 years,[5] the nature of the passage of a many-body quantum system through a CI continues to be a challenging problem. The fact that an accessible CI provides a route to ultrafast interstate transfer on the femtosecond time-scale is of particular importance in chemistry. The presence of a CI has been associated with mechanistic aspects of nonradiative decay scenarios such as photoinduced internal conversion and various other charge transfer processes.[3,4,6–15]

As an evolving quantum system encounters a region of phase space containing a CI, the nonadiabatic (electron-nuclear) coupling becomes extremely important; in fact, at the CI point, the nonadiabatic coupling matrix elements diverge,[16] and the Born-Oppenheimer approximation[5,17] breaks down entirely. The strong coupling generated near the CI mixes the electronic states and creates quantum coherence.

The effect of an environment on quantum coherence is an interesting problem that has relevance for quantum dynamics near a CI in condensed phase or complex molecular systems. Since the simulation of the full quantum dynamics of very large many-body systems is not yet feasible, approximate schemes that are numerically tractable and are able to capture the influence of the environment on the electronic dynamics in these systems have been utilized. Recent studies employing a variety of Markovian and non-Markovian approximate evolution equations have revealed various aspects of the relaxation process from an excited state.[18–20] For example, a Redfield equation analysis[18] of the effects of vibrational damping on electronic decay has shown that there are two major time-scales associated with this process: an initial fast decay of electronic population occurring within less than 100 fs where the majority of the electronic population is transferred, followed by a slower relaxation lasting approximately 1 ps during which vibrational relaxation takes place. Other work on CI systems using the multiconfiguration time-dependent Hartree (MCTDH) method has reproduced spectra for molecules such as pyrazine[21] and provided benchmark data for CIs in general environments,[22] which suggest that very few environmental modes are responsible for the initial decay process, while many more modes may participate in the longer time behavior. Full multiple spawning has been used to investigate isomerization dynamics of large molecules near conical intersections.[3]

In this paper we employ the quantum-classical Liouville (QCL) equation to investigate environmental effects on electronic population transfer. This evolution equation is exact for any quantum subsystem bilinearly coupled to a harmonic bath and provides an accurate description of the dynamics of a quantum subsystem interacting with a general molecular environment whose dynamics can be described by classical mechanics in the absence of coupling to the quantum subsystem. The QCL equation has been derived in various ways (see Ref. 23 for a review with references to the literature on this topic); in particular, it can be derived from a lineariza-

---

[a] Electronic mail: akelly@chem.utoronto.ca.
[b] Electronic mail: rkapral@chem.utoronto.ca.

tion approximation to the path integral representation of the full quantum dynamics.[24,25] The models for conical intersections and their environments used in this study are simple but allow us to extract some general features of how the environment influences the dynamics. No changes to the simulation algorithm are needed for the exploration of more complex and realistic condensed phase environments.

In Sec. II the molecular models involving conical intersections which form the basis for this study are described. These models incorporate the various physical effects that can be induced by an external environment, such as electronic and vibrational dephasing and relaxation.[18,19,26–30] The QCL equation and the method used to simulate it are presented in Sec. III. The results of simulations of the QCL dynamics near conical intersection are given in Sec. IV, while the conclusions of the investigation are summarized in Sec. V.

II. CONICAL INTERSECTION MODELS

We study a number of models that can be used to explore dynamics near conical intersections in molecular systems. We adopt a quantum-classical description where part of the system is treated quantum mechanically and the remainder is treated using classical mechanics. The systems under investigation can be partitioned into a subsystem and bath. The subsystem can be partitioned further into a quantum subsystem and its immediate classical environment. In the models presented below, the quantum subsystem will consist of electronic degrees of freedom of a molecule, the immediate classical environment consists of vibrational or other nuclear degrees of freedom of the molecule, and the bath is the condensed phase solvent in which the dynamics takes place. We treat the immediate environment and the bath classically. Below we use a notation where R_s and R_b denote coordinates of the immediate environment and bath, and $R=(R_s,R_b)$ are the coordinates of the entire environment, immediate environment plus bath.

A. Two-state-two-mode model

A simple two-level-two-mode quantum model for the coupled vibronic states of a linear *ABA* triatomic molecule has been constructed by Ferretti, Lami, and Villiani[26,30] in their exact quantum dynamics study of the CI problem. The nuclei of this symmetric linear molecule are described using two vibrational degrees of freedom: a symmetric stretch, X, the so-called tuning coordinate and an antisymmetric stretch, Y, known as the coupling coordinate. The Ferretti–Lami–Villiani (FLV) electronic Hamiltonian matrix in the diabatic basis that enters in our quantum-classical description is

$$\mathbf{H}_s(R_s,P_s)=\left(\frac{P_X^2}{2M_X}+\frac{P_Y^2}{2M_Y}\right)\mathbf{I}+\mathbf{h}(R_s), \tag{1}$$

where the diagonal matrix elements of $\mathbf{h}$ are

$$h_{00}(R_s)=\tfrac{1}{2}M_X\omega_X^2(X-X_1)^2+\tfrac{1}{2}M_Y\omega_Y^2Y^2,$$

$$h_{11}(R_s)=\tfrac{1}{2}M_X\omega_X^2(X-X_2)^2+\tfrac{1}{2}M_Y\omega_Y^2Y^2+\Delta, \tag{2}$$

and the off-diagonal diabatic coupling matrix elements are

$$h_{01}(R_s)=h_{10}(R_s)=\gamma Y e^{-\alpha(X-X_3)^2}e^{-\beta Y^2}. \tag{3}$$

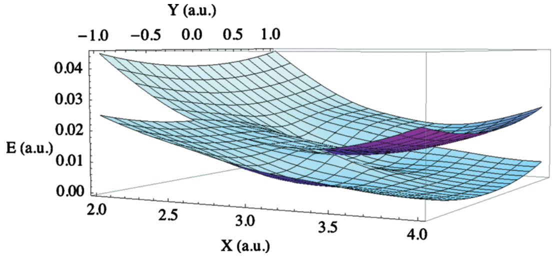

FIG. 1. Plot of the FLV adiabatic electronic energy surfaces for $\gamma=0.02$. The other parameters in the FLV model are $\omega_X=0.001$, $\omega_Y=0.003\,87$, $M_X=20\,000$, $M_Y=6667$, $\alpha=3$, $\beta=1.5$, $X_1=4$, $X_2=X_3=3$, and $\Delta=0.01$, all in atomic units.

In these equations $R_s=(X,Y)$, while $P_s=(P_X,P_Y)$, (M_X,M_Y), and (ω_X,ω_Y) are the momenta, masses, and frequencies corresponding to the X and Y degrees of freedom.

The potential functions describe two shifted two-dimensional parabolic electronic surfaces with an antisymmetric localized coupling. The two diabatic surfaces have minima at $(X_1,0)$ and $(X_2,0)$, respectively, and are degenerate at a single point $(X_3,0)$. The electronic coupling [Eq. (3)] is localized to the region of the intersection by a Gaussian cutoff function which vanishes at large distances from the coupling region and is antisymmetric in the coupling coordinate. The conical intersection coincides with the minimum of the upper diabatic potential surface and is intermediate between a sloped and a peaked crossing.[31] The subsystem adiabatic energies are defined by the eigenvalue problem, $\hat{h}(R_s)|\alpha;R_s\rangle=E_\alpha(R_s)|\alpha;R_s\rangle$, and the adiabatic Born–Oppenheimer energy surfaces, $E_\alpha(R_s)$, are plotted in Fig. 1, which shows the conical intersection between the two surfaces.

The linear vibronic model (LVM)[32,33] is identical in structure to the FLV model but simpler in that it involves linear diabatic coupling terms $(h_{01}=h_{10}=\gamma Y)$. While the diabatic coupling term in the FLV model is localized in the region of the degeneracy, it is global in the LVM model. Electronic structure[13,14] and dynamics[19,20] studies suggest that a localized form for the coupling is more physically relevant in general, as well as the particular case of charge transfer processes. Although the FLV model was originally posited with a small molecule in mind, it has wider physical appeal; in fact this model is similar in form to more complex molecular models which can be treated in terms of coupling and tuning modes. For example, this simple model could be used to capture the essential physical features of charge transfer processes through a conical intersection, between identical moieties in biphenyl-type compounds where the two rings are held at 90° by steric interactions.[34]

The FLV model may be generalized to include coupling to a heat bath by imagining that each of the stretching coordinates experience a further bilinear coupling to identical, but independent, sets of harmonic oscillators. Thus we may include the effect of dissipation on the system in our QCL description. The total Hamiltonian matrix takes the form

$$\mathbf{H}(R,P)=\mathbf{H}_s(R_s,P_s)+\left(\sum_j^{N_B}\frac{P_j^2}{2M_j}+\frac{M_j\omega_j^2}{2}\left(R_j-\frac{c_j}{M_j\omega_j^2}X\right)^2+\sum_l^{N_B}\frac{P_l^2}{2M_l}+\frac{1}{2}M_l\omega_l^2\left(R_l-\frac{c_l}{M_l\omega_l^2}Y\right)^2\right)\mathbf{I}. \quad (4)$$

The coordinates and momenta of each bath oscillator with mass M_j are (R_j,P_j), and N_B is the number of oscillators. The coupling constants and frequencies, c_j and ω_j, are chosen to correspond with those of a harmonic bath with an Ohmic spectral density. For this generalized model the subsystem free energies correspond to the adiabatic potential surfaces of the original FLV model. The degree of dissipation or damping by the bath of the vibrational degrees of freedom is controlled by the Kondo parameter, ξ, in the Ohmic spectral density.[35] In the simulation results presented below we have chosen small to intermediate values of this parameter, such that the effects of damping are important, but that the vibrational system is not highly damped. Although we have limited the scope of our calculations to the Ohmic spectral density here, one may choose any appropriate spectral density to characterize the bath without changing the structure of the above model.

B. Avoided crossing model

By dropping the linear factor in the diabatic coupling term in FLV model, we return to the case of an avoided crossing, where the degeneracy in the diabatic basis is lifted by the transformation to the adiabatic basis. Although the avoided crossing may not necessarily pose the same steep theoretical challenges as the conical intersection, later we shall find it useful for the purpose of comparison. A two-dimensional avoided crossing (AC) model may then be defined in the diabatic basis exactly as per the FLV model with the exception of the diabatic coupling, where we make the substitution

$$h_{01}^{\mathrm{AC}}(R_s)=\gamma e^{-\alpha(X-X_3)^2/\sigma^2}e^{-\beta Y^2/\sigma^2}. \quad (5)$$

The new parameter σ is a measure of the size of the localized coupling region.

C. Two-state-three-mode model

In the generalized FLV model the harmonic bath acts as an unstructured dissipative environment for the quantum subsystem and its immediate environment. In some circumstances, such as quantum processes involving charge transfer in polar media, the solvent can participate in a more intimate way in the dynamics.[27] If the two quantum states of the subsystem have markedly different charge distributions, solvent orientational degrees of freedom can lead to selective solvation of the different charge transfer states and the solvent dynamics then may play an essential role in the quantum dynamics. Often the such solvent effects are captured in a global solvent polarization coordinate that couples to the subsystem degrees of freedom.[27,28,36]

As mentioned previously, the simple FLV model can capture some essential features of an intramolecular charge transfer process involving a conical intersection, given a suitable interpretation for the tuning and coupling modes. Since such charge transfer processes in a polar medium involve coupling to the solvent polarization, we may introduce a polarizationlike coordinate in order to mimic such effects. The effect of this new coordinate, Z, is to shift and modulate the subsystem free energy surfaces in a manner similar to that in more realistic models of charge transfer conical intersection dynamics in polar solvents.

In this model the Hamiltonian takes the form

$$\mathbf{H}(R,P)=\left(\frac{P_X^2}{2M_X}+\frac{P_Y^2}{2M_Y}+\frac{P_Z^2}{2M_Z}\right)\mathbf{I}+\mathbf{h}(R), \quad (6)$$

where $R_s=(X,Y)$ and $R=(X,Y,Z)$, with the matrix elements of $\mathbf{h}$ given explicitly by

$$h_{00}(R)=h_{00}(X,Y)+\tfrac{1}{2}M_Z\omega_Z^2Z^2,$$

$$h_{11}(R)=h_{11}(X,Y)+\tfrac{1}{2}M_Z\omega_Z^2(1-Z)^2+\Delta_Z. \quad (7)$$

The off-diagonal matrix elements are identical to those of the FLV model and are given by Eq. (3). Clearly, we have appropriated the FLV vibronic system and coupled it with a third polarizationlike "solvent" coordinate; for convenience it shall be referred to as the XYZ model. The new polarizationlike coordinate couples slightly differently to each diabatic state; depending on the quantum state of the subsystem the solvent coordinate favors different equilibrium nuclear configurations and thus can cause fluctuations in the energy gap of the subsystem over the course of the dynamics. The XYZ model aims to describe a host of environmental effects on a molecular subsystem containing a conical intersection; the environment induces fluctuations in the adiabatic energy gap giving rise to electronic dephasing and provides vibrational dissipation and dephasing. The addition of the solvent coordinate to the two-dimensional model generates a new nonadiabatic coupling term, and the set of conical intersections in the model corresponds to a linear seam of points in the (X,Z)-plane at $Y=0$.

The polarizationlike coordinate Z represents a single collective coordinate of the many-body solvent. The remaining solvent degrees of freedom, which are assumed to be only weakly coupled to the tuning and coupling coordinates, act as a dissipative bath for the solvent polarization. Thus, this model may be generalized to account for this effect by coupling the polarization coordinate Z to a harmonic bath,

$$\mathbf{H}(R,P)=\left(\frac{P_X^2}{2M_X}+\frac{P_Y^2}{2M_Y}+\frac{P_Z^2}{2M_Z}\right)\mathbf{I}+\mathbf{h}(R)+\left(\sum_j^{N_B}\frac{P_j^2}{2M_j}+\frac{M_j\omega_j^2}{2}\left(R_j-\frac{c_j}{M_j\omega_j^2}Z\right)^2\right)\mathbf{I}. \quad (8)$$

Note that in the above expression the bath modes are now coupled indirectly to the subsystem vibrational coordinates (X,Y) via the solvent coordinate (Z), whereas in the generalized FLV model (4) the bath couples directly to these modes.

III. QUANTUM-CLASSICAL DYNAMICS

The dynamics of the aforementioned model systems will be investigated using the quantum-classical Liouville (QCL) equation. This equation can be represented in any convenient basis and the simulation algorithm for the dynamics depends on the choice of basis.[37] In the adiabatic basis this equation takes the form[38]

$$\frac{\partial}{\partial t}\rho_W^{\alpha\alpha'}(R,P,t) = -i\sum_{\beta\beta'} \mathcal{L}_{\alpha\alpha',\beta\beta'}\rho_W^{\beta\beta'}(R,P,t), \tag{9}$$

where the QCL operator is

$$i\mathcal{L}_{\alpha\alpha',\beta\beta'} = (i\omega_{\alpha\alpha'} + iL_{\alpha\alpha'})\delta_{\alpha\beta}\delta_{\alpha'\beta'} - \mathcal{J}_{\alpha\alpha',\beta\beta'}. \tag{10}$$

Here the subscript W indicates that the equation was derived by considering a partial Wigner transform over the environmental degrees of freedom. The structure of $\mathcal{L}$ given above consists of two distinct components. (i) Classical propagation described by $iL_{\alpha\alpha'}$,

$$iL_{\alpha\alpha'} = \frac{P}{M}\cdot\frac{\partial}{\partial R} + \frac{1}{2}(F_W^{\alpha} + F_W^{\alpha'})\cdot\frac{\partial}{\partial P}, \tag{11}$$

which involves the Hellmann–Feynman forces, $F_W^{\alpha} = -\langle\alpha;R|\partial\hat{V}_W(\hat{q},R)/\partial R|\alpha;R\rangle$. If $\alpha\neq\alpha'$ evolution occurs on the mean of two adiabatic surfaces and is accompanied by quantum mechanical phase oscillations with frequency $\omega_{\alpha\alpha'} = (E_\alpha - E_{\alpha'})/\hbar \equiv E_{\alpha\beta}/\hbar$. (ii) Nonadiabatic transitions are described by the operator $\mathcal{J}$,

$$\begin{aligned}\mathcal{J}_{\alpha\alpha',\beta\beta'} = &-\frac{P}{M}\cdot d_{\alpha\beta}\left(1 + \frac{1}{2}S_{\alpha\beta}\cdot\frac{\partial}{\partial P}\right)\delta_{\alpha'\beta'}\\ &-\frac{P}{M}\cdot d^{*}_{\alpha'\beta'}\left(1 + \frac{1}{2}S^{*}_{\alpha'\beta'}\cdot\frac{\partial}{\partial P}\right)\delta_{\alpha\beta},\end{aligned} \tag{12}$$

where $S_{\alpha\beta} = E_{\alpha\beta}d_{\alpha\beta}((P/M)\cdot d_{\alpha\beta})^{-1}$ and $d_{\alpha\beta} = \langle\alpha;R|\partial/\partial R|\beta;R\rangle$ is the nonadiabatic coupling matrix element. In this formalism nonadiabatic transitions change the quantum state of the subsystem. The momentum derivatives in $\mathcal{J}$ account for the energy transfers to and from the classical degrees of freedom which accompany the change of state in the quantum subsystem.

We are primarily interested in the computation of observables, such as electronic state populations or coherences, as a function of time. The expression for the expectation value of a general observable $\hat{B}_W(R,P)$ is

$$\begin{aligned}\overline{B(t)} &= \mathrm{Tr}'\int dRdP\hat{B}_W(R,P)\hat{\rho}_W(R,P,t)\\ &= \mathrm{Tr}'\int dRdP\hat{B}_W(R,P,t)\hat{\rho}_W(R,P)\\ &= \sum_{\alpha\alpha'}\int dRdPB_W^{\alpha\alpha'}(R,P,t)\rho_W^{\alpha'\alpha}(R,P),\end{aligned} \tag{13}$$

where Tr′ denotes a trace over the states of the quantum subsystem.

Such average values may be simulated by QCL dynamics using a Trotter-based algorithm.[39] To compute the average values in Eq. (13) using this scheme, the environmental phase space points are sampled from distributions determined from $\rho_W^{\alpha\alpha'}(R,P)$ and the quantum states are sampled from a uniform distribution. The time evolution of the operator is simulated by a molecular dynamics-Monte Carlo algorithm. The quantum-classical propagator is written as a product of short time classical evolution segments separated by quantum transitions described by the $\mathcal{J}$ operator. The action of this operator is evaluated in the momentum-jump approximation, and the nonadiabatic events are sampled by a Monte Carlo method. Filtering of the observable is employed in the Monte Carlo estimate of the observable. Full details of the algorithm are described in Refs. 39 and 40.

It was noted earlier that the nonadiabatic coupling matrix elements diverge at the CI so it may seem that an adiabatic basis is not the optimal choice for simulation. In the Trotter-based algorithm these coupling elements appear in bounded trigonometric functions. Very large values of the coupling that arise in a very small neighborhood of the CI do lead to oscillations in the observable that make sampling more difficult for such phase space points. However, since average values like those in Eq. (13) are being computed and only very small fraction of the ensemble of trajectories used to simulate the average experience such variations, expectation values can be computed reliably as the data below will demonstrate.

Since the QCL equation is exact for any quantum system bilinearly coupled to harmonic degrees of freedom, it is exact for spin-boson-type models. The FLV model and its variants provide a more stringent test of the QCL theory since the Gaussian cutoff on h_{01} produces an infinite set of higher-order terms in the full quantum propagator, which are treated approximately in the QCL theory. In contrast, the QCL equation is exact for the LVM, and the short time dynamics of this model has been studied.[11]

IV. DYNAMICS SIMULATIONS

We consider the dynamics of these systems starting from an initial state corresponding to a Gaussian wave packet on the excited state adiabatic surface. We assume Feynman–Vernon-type initial conditions where the initial density may be decomposed into electronic subsystem and environmental (vibrational and bath) components, $\hat{\rho}_W(R,P) = \hat{\rho}_s\rho_W^{(\mathrm{vib})}\times(R_s)\rho_W^{(b)}(R_b,P_b)$. The initial vibrational states are chosen to be Gaussian wave packets. For the two-mode models we have

$$\psi^{(\mathrm{vib})}(R_s) = \frac{1}{\sqrt{\pi\Delta_X\Delta_Y}}e^{-(X-X_0)^2/\Delta_X^2}e^{-Y^2/\Delta_Y^2}, \tag{14}$$

while for the three-mode model we have

$$\begin{aligned}\psi^{(\mathrm{vib})}(R_s) = &\frac{1}{\sqrt{\pi^{3/2}\Delta_X\Delta_Y\Delta_Z}}e^{-(X-X_0)^2/\Delta_X^2}\\ &\times e^{-Y^2/\Delta_Y^2}e^{-(Z-Z_0)^2/\Delta_Z^2}.\end{aligned} \tag{15}$$

These initial wave packets are then Wigner transformed,

$$\rho_W^{(\mathrm{vib})}(R_s,P_s) = (2\pi\hbar)^{-N}\int dz e^{iP_s\cdot z/\hbar}\psi^{*(\mathrm{vib})}\left(R_s-\frac{z}{2}\right) \times \psi^{(\mathrm{vib})}\left(R_s+\frac{z}{2}\right), \qquad (16)$$

in order to obtain the initial densities.

The harmonic bath is described by an Ohmic spectral density,[35]

$$J(\omega) = \pi\sum_{j=1}^{N_B} c_j^2/(2M_j\omega_j)\,\delta(\omega-\omega_j), \qquad (17)$$

where $c_j=(\xi\hbar\omega_0 M_j)^{1/2}\omega_j$, $\omega_j=-\omega_c\ln(1-j\omega_0/\omega_c)$, and $\omega_0=\omega_c(1-e^{-\omega_{\max}/\omega_c})/N_B$. The oscillator baths are assumed to initially be in thermal equilibrium, and we adopt the quantum bath distribution function,[41]

$$\rho_W^{(b)}(R,P) = \prod_j \frac{\tanh(\beta\omega_j/2)}{\pi}\exp\left[-\frac{2\tanh(\beta\omega_j/2)}{\omega_j} \times \left(\frac{P_j'^2}{2}+\frac{\omega_j^2 R_j'^2}{2}\right)\right], \qquad (18)$$

where $(R_j',P_j')=(R_j-(c_j/\omega_j^2)X,P_j)$. The classical heat bath is characterized by three parameters: the frequency ω_c, the Kondo parameter ξ, and the dimensionless reciprocal temperature $\beta=\hbar\omega_c/k_BT$. The frequency ω_c determines the peak and width of the Ohmic spectral density and defines the characteristic time-scale of the bath dynamics. The Kondo parameter determines the amplitude of the spectral density and the coupling strengths to the nuclear coordinates. The effects of finite temperature in this model arise in the widths of the initial distributions for the coordinates and momenta of the bath. In the simulations presented here, $N_B=100$ for each set of oscillators, and $\omega_{\max}=3\omega_c$. We have chosen β at room temperature corresponding to $T=300$ K.

The adiabatic ground and excited state populations, P_{S_0} and P_{S_1}, respectively, are given by

$$P_{S_{\alpha''}}(t) = \mathrm{Tr}'\int dRdP\hat{P}_{S_{\alpha''}}(R_s)\hat{\rho}_W(R,P) = \sum_{\alpha\alpha'}\int dRdPP_{S_{\alpha''}}^{\alpha\alpha'}(R,P,t)\rho_W^{\alpha'\alpha}(R,P), \qquad (19)$$

which has the same form as the expectation value for a general operator considered in Eq. (13). The projector onto the adiabatic state α'' is $\hat{P}_{S_{\alpha''}}(R_s)=|\alpha'';R_s\rangle\langle\alpha'';R_s|$ and $P_{S_{\alpha''}}^{\alpha\alpha'}(R_s)=\delta_{\alpha\alpha''}\delta_{\alpha'\alpha''}$. We shall also compute other quantities such as the reduced subsystem densities,

$$\rho_s^{\alpha\alpha}(R_s,t) = \int dP_s dR_b dP_b \rho_W^{\alpha\alpha}(R,P,t), \qquad (20)$$

and the electronic coherence,

$$\rho_s^{01}(t) = \int dRdP\rho_W^{01}(R,P,t). \qquad (21)$$

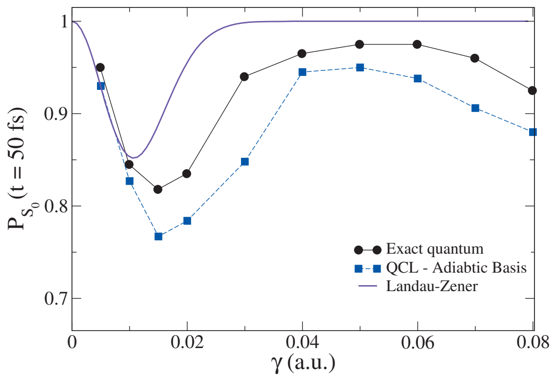

FIG. 2. Adiabatic ground state population after the system has made a single pass through the CI region $P_{S_0}(t=50\text{ fs})$ vs γ for the gas phase FLV model.

A. Population dynamics

The ground state population after the system has made a single pass through the CI region, $P_{S_0}(t=50\text{ fs})$, and is shown in Fig. 2 as a function of the coupling strength γ for the simple gas phase FLV model. The QCL equation results are compared with exact quantum dynamics,[26] and the Landau–Zener approximation. The results in this figure indicate that QCL dynamics provides a good approximation to the full quantum dynamics. It is numerically exact at low γ and is a good approximation to the exact results over the full range of γ. It is able to describe the trends seen in $P_{S_0}(t=50\text{ fs})$ versus γ better than the simple Landau–Zener estimate.

The effect of a bath on the population dynamics can be seen in Fig. 3, which plots the population of the adiabatic ground state as a function of time for the generalized FLV model for a range of dimensionless bath frequencies, ω_c, with fixed low values of the Kondo parameter and coupling strength. [Here and in the remainder of this section, ω_c and ω_Z are reported in units of ω_X, i.e., $(\omega_c\to\omega_c/\omega_X$, $\omega_Z\to\omega_Z/\omega_X)$, since the bath frequency relative to that of the oscillator determines the character of the dynamics.] For low electronic coupling strength and weak damping, we see that the system experiences greater population transfer to the ground state when a bath is present than when it is absent.

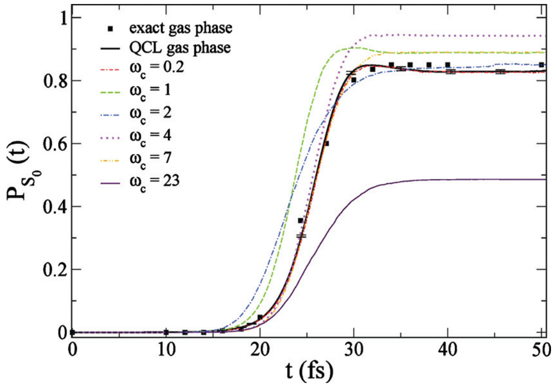

FIG. 3. Ground adiabatic state population $P_{S_0}(t)$ vs time for $X_0=2$, $\gamma=0.01$, $\xi=0.1$, and a range of different bath characteristic frequencies, ω_c, reported in units of ω_X. The solid squares are the exact quantum results for the gas phase model. Note that QCL dynamics is in close accord with the exact gas phase results over the entire time range.

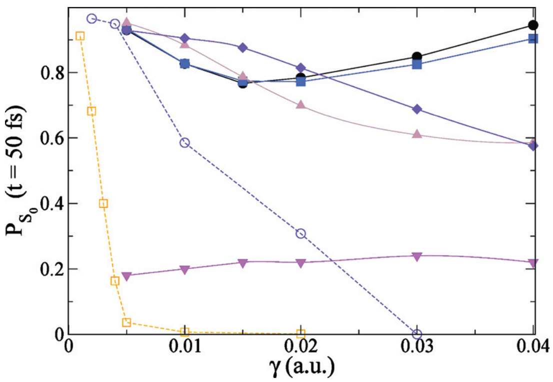

FIG. 4. Ground adiabatic state populations $P_{S_0}(t=50\ \text{fs})$ vs γ with $\xi=0.1$, for a range of different bath characteristic frequencies, ω_c, in units of ω_X. FLV model (solid symbols and lines), gas phase (squares), $\omega_c=0.2$ (circles), $\omega_c=1$ (up-triangles), $\omega_c=4$ (diamonds), and $\omega_c=23$ (down-triangles). AC model (open symbols, dotted lines), gas phase (squares), and $\omega_c=2$ (circles).

Such enhancement of population transfer due to interaction with an environment has been observed in earlier studies of environmental effects on dynamics near a conical intersection.[18,20] This enhancement effect is seen for all but the highest characteristic frequency reported in Fig. 3. The population transfer is suppressed for bath frequencies that are significantly higher than the nuclear vibration frequencies. (For reference the oscillator frequencies in the original FLV model[26] in dimensional units are $\omega_X=219\ \text{cm}^{-1}$ and $\omega_Y=850\ \text{cm}^{-1}$.)

The population transfer to the ground state is enhanced for a range of low coupling strengths and for bath frequencies from 0.2 to 4. However, for these bath frequencies, the population transfer is a decreasing function of γ, which somewhat follows the shape of the bath-free curve. For moderate coupling strengths $(\gamma > 0.02)$, in Fig. 4 we see that the population transfer is suppressed for all but the smallest bath frequencies simulated. When the bath dynamics becomes very fast relative to that of the subsystem $(\omega_c=23)$, the population transfer is heavily suppressed for all (γ,ξ) studied. In this case the transfer ratio is relatively insensitive to the electronic coupling strength.

For the AC model, the population transfer to the ground state monotonically decreases as a function of the electronic coupling strength. These results are also shown in Fig. 4. Clearly this behavior is different than in the conical intersection model, where the population transfer increases for higher coupling strengths. The population transfer also decays as a function of γ in the case of a moderately fast bath (Fig. 4); however, the population transfer decreases less steeply as a function of γ than for the gas phase AC model. This effect is similar to that seen in the generalized FLV conical intersection model, where for low coupling strength the population transfer is higher than the gas phase case for moderate bath frequencies.

It is also interesting to compare the results obtained using QCL dynamics with the well-known surface-hopping dynamics method, based on Tully's fewest-switches algorithm.[42] Figure 5 shows that in the gas phase the QCL and surface-hopping results agree at low electronic coupling strengths but differ substantially at large coupling strengths.

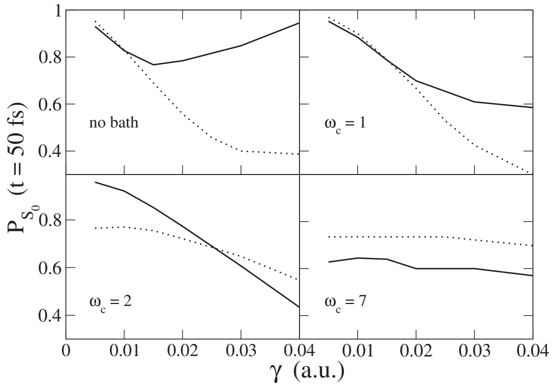

FIG. 5. Ground adiabatic state population $P_{S_0}(t=50\ \text{fs})$ for a range of coupling strengths γ, and bath characteristic frequencies, ω_c, reported in units of ω_X, with $\xi=0.1$. The solid lines are the QCL results and the dotted lines correspond to surface-hopping results generated using Tully's method.

For cases where the bath is present the surface-hopping and QCL results are in closer accord, even for large coupling strengths even though discrepancies exist in all parameter ranges studied. The fact that results show better overall agreement with bath present may be an indication that the bath provides a mechanism for decoherence so that a simple surface-hopping scheme may be more easily justified.

Next, we consider the three-mode XYZ model in the case that the coupling to the solvent coordinate is considerable.[27,36] We investigate a range of solvent frequencies, ω_Z; in the contrasting cases of a fast or slow solvent, shown in Fig. 6, we see that the population transfer profile in the three-mode model is quite sensitive to the frequency of the Z oscillator. In the case of a sluggish Z coordinate the transition is almost completely suppressed over the initial portion of the dynamics. As ω_Z becomes comparable to the nuclear vibrational frequencies the ultrafast transition does indeed occur. However, if the solvent coordinate is subsequently coupled to a dissipative heat bath with a relatively fast characteristic frequency $(\omega_c=7)$, the transition is strongly suppressed over the initial portion of the dynamics.

B. Purity and electronic coherence

The effects of decoherence by the bath can be seen by examining the purity, $\text{Tr}'\hat{\rho}_s(t)^2$, shown in Fig. 7, or the off-

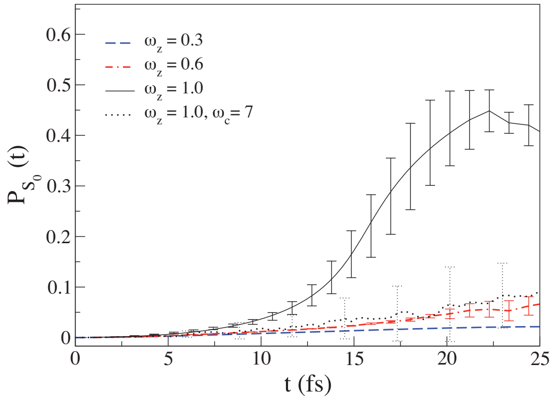

FIG. 6. Ground state population as a function of time in the XYZ model, for $Z_0=0$, $\gamma=0.005$, $\Delta_Z=0$, and $M_Z\omega_Z^2=0.092$ (2.5 eV). In the case with the bath present, $\xi=1$.

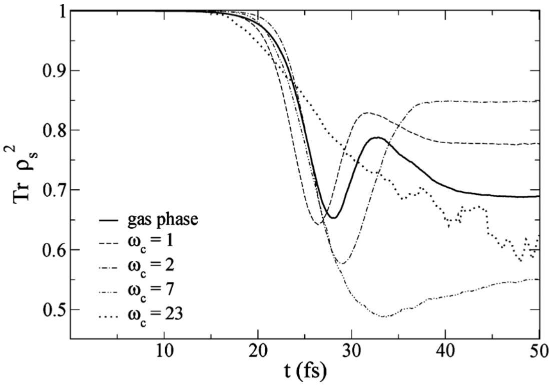

FIG. 7. Purity, $\mathrm{Tr}'\hat{\rho}_s(t)^2$, of the quantum subsystem as a function of time, for several characteristic bath frequencies, for $\gamma=0.01$.

diagonal element of the quantum subsystem density matrix $\rho_s^{01}(t)$, shown in Fig. 8. As one might expect from the population transfer results, there is an increase in the purity after a single pass through the intersection for most characteristic bath frequencies when the electronic coupling is weak due to the enhanced transfer to the ground state. However, once the bath dynamics becomes much faster than that of the subsystem, the purity decays monotonically with time (cf. results for $\omega_c=23$). It is also evident that, by increasing the characteristic frequency of the bath, the envelope of coherence oscillations, which are induced during motion through the region of the conical intersection, decays more rapidly.

It has been shown in other model studies[19,20] that a narrow avoided crossing may cause the system to evolve in a manner somewhat similar to that for a true conical intersection. This situation may be investigated by narrowing the diabatic coupling function, i.e., by reducing the value of σ in Eq. (5). One can see from Fig. 8 for the bath-free system with the original coupling width ($\sigma=1$, regular width) that the evolution of the electronic coherence does not resemble that for the FLV system. In contrast, it is evident that when a bath is present, or the width of the coupling is reduced ($\sigma=\frac{1}{2}$, half-width), the coherence indeed resembles that of the FLV system. However, the quantum coherence generated in the avoided crossing system is more sensitive to the presence of the bath than in the case of its conical intersection counterpart.

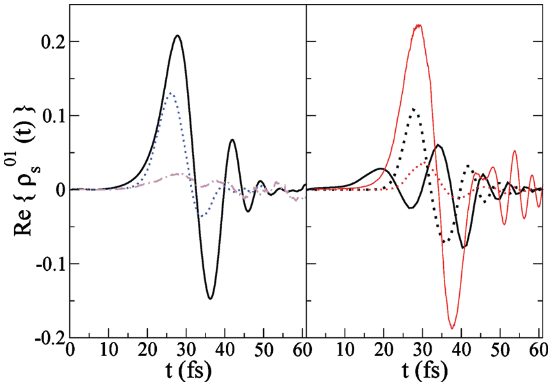

FIG. 8. Evolution of the electronic coherence as a function of time. Left panel: FLV model results; gas phase (full line), $\omega_c=2$ (dotted line), and $\omega_c=23$ (dotted-dashed line). Right panel: ACM with $\sigma=1$; gas phase (heavy line), $\omega_c=2$ (heavy dotted line), and $\sigma=1/2$ gas phase (thin line) and $\omega_c=2$ (thin dotted line). In all cases $\gamma=0.01$ and for cases with the bath present $\xi=1$.

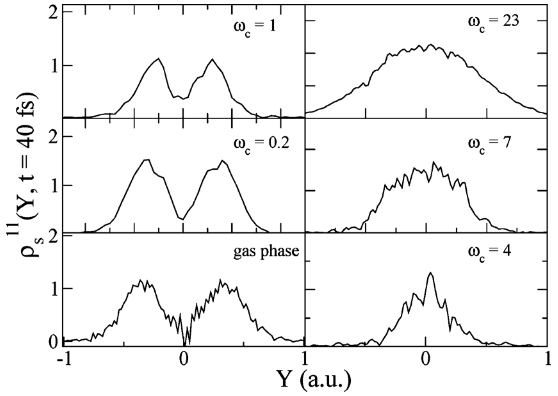

FIG. 9. Destruction of the node in the subsystem reduced density along the Y coordinate, as a function of ω_c, in units of ω_X, from QCL simulations.

C. Geometric phase

One important consequence of the presence of a conical intersection on the potential energy landscape is the emergence of a geometric (Berry) phase.[43,44] In the FLV model the evidence of a Berry phase in the system arises as a nodal structure in the subsystem excited state density projected along the Y-coordinate.[26,45] The reproduction of this delicate quantum phenomenon provides an important challenge to any approximate theory and its accompanying simulation algorithm. At low coupling strengths, this effect manifests as a single node in the excited state density at $Y=0$, a feature that is well reproduced by the QCL simulations in the adiabatic basis. For larger values of γ this interference pattern becomes more complicated. The Landau–Zener approximation and surface-hopping dynamics[42] schemes are incapable of reproducing this structure.[26] Earlier QCL calculations in the force basis were able to capture aspects of this delicate feature.[46] As shown in Fig. 9, the Trotter-based QCL simulations are indeed able to reproduce this feature. In addition, Fig. 9 shows the gradual destruction of this node as the bath frequency increases in the generalized FLV model.

It is also interesting to see if nodal structure, or other interference phenomena, arises as consequence of the geometric phase in the other models considered in this paper. In particular, in the three-mode model there is a seam of intersections, as opposed to a conical intersection at a single point in configuration space. A significant shift in the interference pattern is expected for this model and, indeed, we see in Fig. 10 that there is no node at $Y=0$ in the subsystem excited state coordinate distribution after the system has passed through the CI region. While no node due the geometric phase effect is expected for the AC model, we find that a minimum appears at $Y=0$ when the electronic coupling region is made more narrow (cf. Fig. 10).

V. CONCLUSION

Recent research on the dynamics of systems with conical intersections, which has been driven by the ubiquity and im-

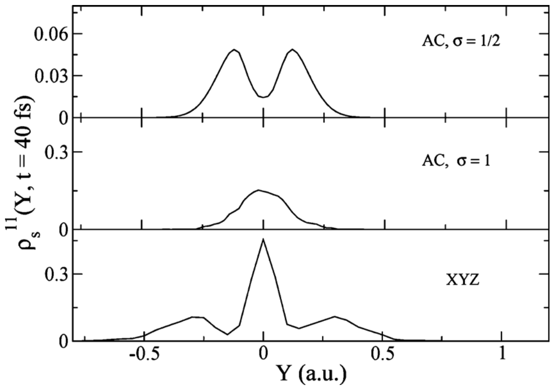

FIG. 10. Subsystem density in the excited state as a function of the Y coordinate, for QCL simulations of the AC model with $\sigma=1$, and $\sigma=1/2$, and the XYZ model for weak coupling to a slow solvent coordinate, $\omega_Z=0.3$.

portance of CI phenomena in chemical systems, has increased greatly since the early work on this topic. The quantum coherence generated in CI quantum dynamics can serve as a paradigm for our fundamental understanding of other coherently coupled systems.

The results of investigations of the effects of an external environment on the electronic dynamics in model molecular systems containing conical intersections and avoided crossings described in this paper have shown that the population transfer may be enhanced or suppressed, depending on the relative values of the characteristic frequencies of the subsystem and environment. Electronic decoherence and the destruction of geometric phase effects were observed as the external degrees of freedom became fast relative to the molecular vibrations. The environmental effects come into play in various forms.[1–4] The molecular vibrational degrees of freedom act as bath on the electronic degrees of freedom; in addition, other solvent degrees of freedom also play the role of a dissipative environment that influences the population dynamics. The models studied in this paper have allowed us to consider some aspects of the distinctive features that arise from different bath characteristics as seen, for example, in the comparisons between the FLV and XYZ model results where the bath descriptions have different characteristics.

In accord with earlier work,[20] we also found that the dynamics at a narrow avoided crossing may mimic some aspects of the dynamics near a conical intersection; however, the dynamics through a CI in the presence of an environment was shown to behave quite differently from that of an avoided crossing. Further, the dynamics at higher dimensional CIs was shown to be highly sensitive to the environmental coupling. In the simple case where a single collective solvent coordinate couples directly to the electronic subsystem, the characteristic frequency of the new coordinate (relative to that of the nuclear vibrational modes), was shown to have a strong impact on the short time dynamics. In addition, we showed that the presence of a dissipative environment may also strongly alter the short time electronic dynamics through indirect coupling via the solvent mode.

While the conical intersection models and descriptions of the environmental degrees of freedom considered here were simple, our interest is in the description in the dynamics realistic molecular models for condensed phase systems. Quantum-classical descriptions of the dynamics provide the possibility to simulate the evolution of such large many-body systems when the environmental degrees of freedom can be treated classically to a good approximation. In this connection another goal of this investigation was the exploration of the utility of the QCL equation as the dynamical basis for condensed phase conical intersection dynamics. The results presented in the paper showed that QCL dynamics is in good agreement with the exact quantum results for the gas phase FLV model and provides a more accurate description than simple surface-hopping schemes. While the Trotter-based algorithm was used to simulate the dynamics of our model systems, the same algorithm can be applied directly to simulations where the environment is described at a detailed molecular level.

Since the simulation method depends on the choice of basis for the representation of the quantum degrees of freedom in the QCL equation, it is likely that other choices, such as those based on the mapping Hamiltonian method currently under study,[47] may lead to even more effective simulation algorithms for dynamics near conical intersections that avoid some of the difficulties associated with Monte Carlo sampling of the quantum transitions.

ACKNOWLEDGMENTS

This work was supported in part by a grant from the Natural Sciences and Engineering Research Council of Canada.

[1] D. R. Yarkony, Rev. Mod. Phys. **68**, 985 (1996).
[2] G. Worth and L. Cederbaum, Annu. Rev. Phys. Chem. **55**, 127 (2004).
[3] B. G. Levine and T. Martínez, Annu. Rev. Phys. Chem. **58**, 613 (2007).
[4] *Conical Intersections: Electronic Structure, Dynamics and Spectroscopy*, edited by W. Domcke, D. R. Yarkony, and H. Köppel (World Scientific, Singapore, 2004).
[5] E. Teller, J. Phys. Chem. **41**, 109 (1937).
[6] M. Robb, F. Bernardi, and M. Olivucci, Pure Appl. Chem. **67**, 783 (1995).
[7] *Femtochemistry*, edited by F. D. Schryver, S. D. Feyter, and G. Schweitzer (Wiley-VCH, Germany, 2001).
[8] V. Bonačić-Koutecký, J. Koutecky, and J. Michl, Angew. Chem., Int. Ed. Engl. **26**, 170 (1987).
[9] J. Tennyson and J. Murrell, Nouv. J. Chim. **5**, 361 (1981).
[10] M. Thoss, W. Miller, and G. Stock, J. Chem. Phys. **112**, 10282 (2000).
[11] G. Stock and M. Thoss, Adv. Chem. Phys. **131**, 243 (2005).
[12] P. Celani, F. Bernardi, M. Olivucci, and M. Robb, J. Am. Chem. Soc. **119**, 10815 (1997).
[13] M. Garavelli, P. Celani, F. Bernardi, M. Robb, and M. Olivucci, J. Am. Chem. Soc. **119**, 6891 (1997).
[14] M. J. Thompson, D. Bashford, L. Noodleman, and E. D. Getzoff, J. Am. Chem. Soc. **125**, 8186 (2003).
[15] *Quantum Dynamics at Conical Intersections Collaborative Computational Project on Molecular Quantum Dynamics (CCP6)*, edited by S. Althorpe and G. Worth (Computational Project 6, United Kingdom, 2004).
[16] H. Köppel, W. Domcke, and L. Cederbaum, Adv. Chem. Phys. **57**, 59 (1984).
[17] M. Born and I. Oppenheimer, Ann. Phys. **389**, 457 (1927).
[18] A. Kühl and W. Domcke, Chem. Phys. **259**, 227 (2000).
[19] G. Katz, R. Kosloff, and M. Ratner, Isr. J. Chem. **44**, 53 (2004).
[20] D. Gelman, G. Katz, R. Kosloff, and M. Ratner, J. Chem. Phys. **123**, 134112 (2005).
[21] A. Raab, G. Worth, H. Meyer, and L. Cederbaum, J. Chem. Phys. **110**, 936 (1999).
[22] L. S. Cederbaum, E. Gindensperger, and I. Burghardt, Phys. Rev. Lett.

94, 113003 (2005).

[23] R. Kapral, Annu. Rev. Phys. Chem. **57**, 129 (2006).

[24] S. Bonella, G. Ciccotti, and R. Kapral, Chem. Phys. Lett. **484**, 399 (2010).

[25] Q. Shi and E. Geva, J. Chem. Phys. **120**, 10647 (2004).

[26] A. Ferretti, G. Granucci, A. Lami, M. Persico, and G. Villani, J. Chem. Phys. **104**, 5517 (1996).

[27] I. Burghardt, L. S. Cederbaum, and J. T. Hynes, Faraday Discuss. **127**, 395 (2004).

[28] I. Burghardt and J. T. Hynes, J. Phys. Chem. A **110**, 11411 (2006).

[29] A. Ferretti, A. Lami, and G. Villani, J. Chem. Phys. **107**, 3498 (1997).

[30] A. Ferretti, A. Lami, and G. Villani, J. Chem. Phys. **106**, 934 (1997).

[31] G. J. Atchity, S. S. Xantheas, and K. Ruedenberg, J. Chem. Phys. **95**, 1862 (1991).

[32] L. S. Cederbaum, W. Domcke, H. Köppel, and W. von Niessen, Chem. Phys. **26**, 169 (1977).

[33] L. S. Cederbaum and W. Domcke, Adv. Chem. Phys. **36**, 205 (1977).

[34] A. Ferretti, A. Lami, and G. Villani, Chem. Phys. **259**, 201 (2000).

[35] K. Thompson and N. Makri, J. Chem. Phys. **110**, 1343 (1999).

[36] I. Burghardt, L. S. Cederbaum, and J. T. Hynes, Comput. Phys. Commun. **169**, 95 (2005).

[37] R. Grunwald, A. Kelly, and R. Kapral, in *Energy Transfer Dynamics in Biomaterial Systems*, edited by I. Burghardt (Springer, Berlin, 2009), pp. 383–413.

[38] R. Kapral and G. Ciccotti, J. Chem. Phys. **110**, 8919 (1999).

[39] D. Mac Kernan, G. Ciccotti, and R. Kapral, J. Phys. Chem. B **112**, 424 (2008).

[40] S. Bonella, D. Coker, D. MacKernan, R. Kapral, and G. Ciccotti, in *Energy Transfer Dynamics in Biomaterial System*, edited by I. Burghardt (Springer, Berlin, 2009), pp. 415–436.

[41] K. Imre, E. Ozizmir, M. Rosenbaum, and P. F. Zweifel, J. Math. Phys. **8**, 1097 (1967).

[42] J. C. Tully, J. Chem. Phys. **93**, 1061 (1990).

[43] M. Berry, Proc. R. Soc. London, Ser. A **392**, 45 (1984).

[44] J. Anandan, Nature (London) **360**, 307 (1992).

[45] J. Schön and H. Köppel, Chem. Phys. Lett. **231**, 55 (1994).

[46] C. C. Wan and J. Schofield, J. Chem. Phys. **116**, 494 (2002).

[47] A. Kelly, R. van Zon, J. Schofield, and R. Kapral (unpublished).